Supplementary Information

Steric trapping reveals a cooperativity network in the intramembrane protease GlpG

Ruiqiong Guo[1,5], Kristen Gaffney[2,5], Zhongyu Yang[3,4], Miyeon Kim[1], Suttipun Sungsuwan[1], Xuefei Huang[1], Wayne L. Hubbell[3] and Heedeok Hong[1,2*]

[1]Department of Chemistry & [2]Department of Biochemistry and Molecular Biology, Michigan State University, East Lansing, MI 48824, USA

[3]Jules Stein Eye Institute and Department of Chemistry and Biochemistry, University of California, Los Angeles, CA 90095, USA

[4]Present Address: Department of Chemistry and Biochemistry, North Dakota State University, Fargo, ND 58102, USA

[5]These authors equally contributed to this work.

Corresponding author:

Heedeok Hong

E-mail: honghd@msu.edu

Tel: 1-517-355-9715 Ext. 352

Supplementary Results

Supplementary Table 1 Stability changes induced by single substitutions and activities of singly-substituted variants in the backgrounds of double-biotin GlpG variants $95/172_N$-$BtnPyr_2$ and $172/267_C$-$BtnPyr_2$. Stabilities were measured by steric trapping in pH 7.0 sodium phosphate, 200 mM NaCl, 0.25 mM TCEP, and 5 mM DDM solution. To calculate the stability change for each substitution, $\Delta G^o_{U,95/172_N\text{-}BtnPyr_2}$=5.8±0.2 kcal/mol and $\Delta G^o_{U,172/267_C\text{-}BtnPyr_2}$=4.7±0.1 kcal/mol were used as wild-type stabilities. Energy values are in kcal/mol. Activity values are relative to wild-type GlpG. $\Delta\Delta\Delta G^o_U$ is defined as $\Delta G^o_{U,\ 95/172_N\text{-}BtnPyr_2} - \Delta G^o_{U,\ 172/267_C\text{-}BtnPyr_2}$. Errors denote propagated s. d. calculated from s. d. of individual ΔG^o_U values.

Mutation	$95/172_N$-$BtnPyr_2$		$172/267_C$-$BtnPyr_2$		$\Delta\Delta\Delta G^o_U$	Location
	$\Delta\Delta G^o_{U,95/172_N\text{-}BtnPyr_2}$ (WT-Mut)	Activity	$\Delta\Delta G^o_{U,172/267_C\text{-}BtnPyr_2}$ (WT-Mut)	Activity		
Cooperative interactions						
M100A	2.8±0.2	0.95 ±0.03	2.5±0.5	0.89 ±0.02	0.3±0.5	Subdomain I[a] TM1[b]/Interface[c]
L161A	1.9±0.2	0.13 ±0.02	1.8±0.4	0.10 ±0.01	0.1±0.4	Subdomain I TM2/Interface
L174A	3.8±0.2	0.23 ±0.04	3.3±0.2	0.14 ±0.05	0.5±0.2	Subdomain I TM3/Interface
T178A	0.7±0.1	1.35 ±0.05	0.3±0.1	1.63 ±0.05	0.5±0.1	Subdomain I TM3/Interface
S201T	1.0±0.2	0.04 ±0.02	1.0±0.3	0.03 ±0.02	0.0±0.4	Subdomain II TM4/Interface
Localized interactions in Subdomain I						
C104A	2.2±0.3	0.81 ±0.02	0.2±0.2	1.30 ±0.04	2.0±0.3	Subdomain I TM1/interface
Y138F	1.9±0.2	0.59 ±0.03	0.6±0.2	1.48 ±0.04	1.3±0.4	Subdomain I L1
T140A	1.7±0.1	1.39 ±0.05	0.7±0.2	1.19 ±0.04	0.9±0.2	Subdomain I L1
L143A	2.4±0.2	0.96 ±0.02	1.3±0.2	1.26 ±0.03	1.1±0.2	Subdomain I L1
N154A	1.3±0.2	0.07 ±0.01	0.4±0.3	0.09 ±0.01	0.9±0.2	Subdomain I TM2/interface
W158F	1.1±0.2	1.41 ±0.05	0.1±0.2	1.27 ±0.04	1.0±0.3	Subdomain I TM2/interface
L207A	4.1±0.1	0.08 ±0.01	2.7±0.1	0.08 ±0.02	1.4±0.1	Subdomain II TM4/interface
Y210F	2.0±0.2	1.15 ±0.04	1.3±0.1	0.68 ±0.02	0.7 ±0.2	Subdomain II TM4/Interface

Continued on the next page.

Continued from the previous page.

Mutation	$95/172_N$-$BtnPyr_2$ $\Delta\Delta G^o_{U,95/172_N\text{-}BtnPyr_2}$ (WT-Mut)	Activity	$172/267_C$-$BtnPyr_2$ $\Delta\Delta G^o_{U,172/267_C\text{-}BtnPyr_2}$ (WT-Mut)	Activity	$\Delta\Delta\Delta G^o_U$	Location
Localized interactions in Subdomain II						
L225A	−0.6±0.2	0.28 ±0.05	1.2±0.4	0.33 ±0.04	−1.8±0.4	Subdomain II TM5/Interface
Q226A	−0.2±0.2	1.42 ±0.06	0.8±0.4	1.81 ±0.09	−1.0±0.3	Subdomain II TM5
S181A	−0.5±0.2	1.30 ±0.04	0.6±0.2	1.49 ±0.06	−1.1±0.2	Subdomain I TM3/Interface
Localized interactions in Subdomain I at the TM4/TM6 interface						
A253V	1.7±0.2	0.04 ±0.01	0.8±0.2	0.06 ±0.01	0.9 ±0.3	Subdomain II TM6/Interface
G261A*	4.1±0.2	0.06 ±0.05	2.7±0.2	0.00 ±0.05	1.4 ±0.2	Subdomain II TM6
A265V*	2.4±0.2	0.40 ±0.05	1.3±0.2	0.22 ±0.05	1.1 ±0.3	Subdomain II TM6
D268A	2.5±0.2	0.17 ±0.02	1.3±0.1	0.44 ±0.02	1.2 ±0.2	Subdomain II TM6/Interface

[a]Subdomain in which a mutated residue is located.
[b]Secondary structural elements in which a mutated residue is located.
[c]If a mutated residue is making more than one side-chain contacts with residues in both subdomains, the residue is designated to be located at the subdomain interface.
* Over-propagated interactions

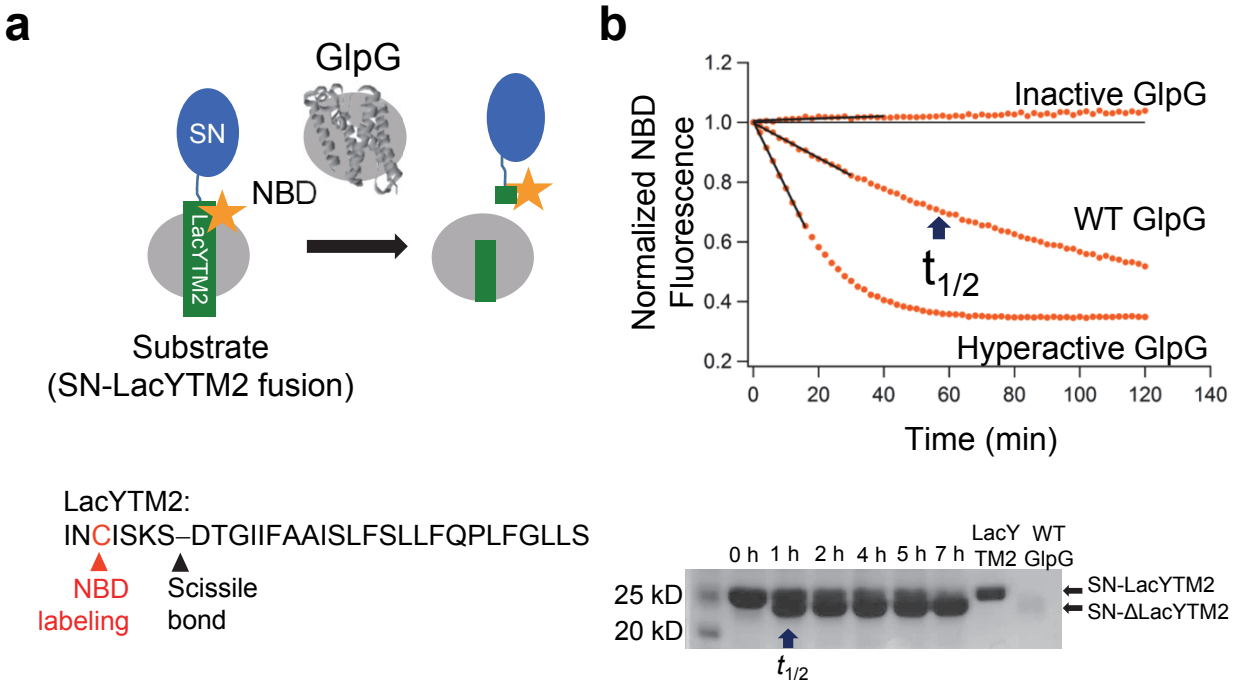

Supplementary Figure 1 | New high-throughput assay for measuring the proteolytic activity of GlpG. (a) Second transmembrane segment of the lactose permease of *E. coli* fused to staphylococcal nuclease domain (SN-LacYTM2) (Akiyama & Maegawa **2007** *Mol Microbiol.* 64, 1028-1037). IA-NBD, a thiol-reactive environment-sensitive fluorophore was conjugated to an engineered cysteine in the P5 position from the scissile bond. Cleavage of LacYTM2 led to a large decrease in the fluorescence intensity as NBD was transferred from the nonpolar micellar phase into the bulk aqueous phase. **(b)** (**Top**) Changes in the NBD fluorescence over time due to the proteolytic activity of GlpG. Addition of wild-type (WT) GlpG decreased NBD fluorescence. In contrast, addition of inactive GlpG variant (S201T) displayed negligible change in NBD fluorescence, and hyperactive GlpG mutant (W236A) increased the rate of NBD fluorescence change relative to WT. (**Bottom**) In the conventional SDS-PAGE assay for GlpG activity, a lower molecular weight band appeared, which corresponded to cleaved SN-LacYTM2 (SN-ΔLacYTM2). For WT GlpG, the half-life ($t_{1/2}$) of the substrate estimated by SDS-PAGE was similar to that measured by the NBD fluorescence change.

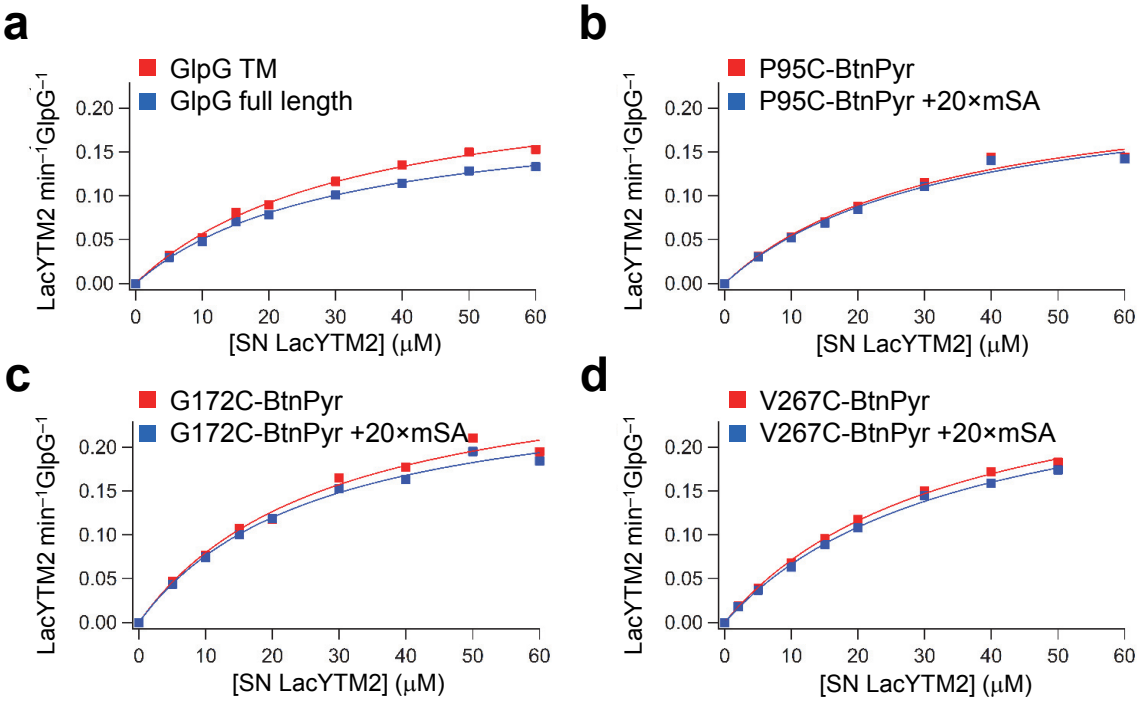

e

	K_M (μM)	k_{cat} (min^{-1})	k_{cat}/K_M (min^{-1} μM^{-1})
WT full length	30±2	0.20±0.01	0.0074±0.0007
WT TM	33±3	0.24±0.01	0.0067±0.0005
P95C-BtnPyr	33±7	0.24±0.03	0.0072±0.0017
P95C-BtnPyr+mSA	34±6	0.23±0.02	0.0070±0.0015
G172C-BtnPyr	29±5	0.31±0.02	0.011±0.0020
G172C-BtnPyr+mSA	27±4	0.28±0.02	0.010±0.0015
V267C-BtnPyr	34±2	0.31±0.01	0.0092±0.0007
V267C-BtnPyr+mSA	35±3	0.30±0.01	0.0082±0.0008

Supplementary Figure 2 | Michaelis-Menten analysis of the proteolytic activity of GlpG. (a) Comparison of GlpG activity of the full-length wild type and the transmembrane domain (TM). **(b)–(d)** Binding of monovalent streptavidin (mSA) to a single BtnPyr label at each site did not affect the activity of GlpG. All measurements were done in pH 7.5 sodium phosphate, 200 mM NaCl, 0.5 mM TCEP , 5 mM n-dodecyl-β-D-maltoside (DDM) detergent solution ([GlpG]=1 μM and [SN-LacYTM2]=20 μM). **(e)** Summary of fitted parameters from Michaelis-Menten analysis of the kinetic activity data. The errors denote mean ± s. d. from the fitting of the data in **(a)**-**(d)**.

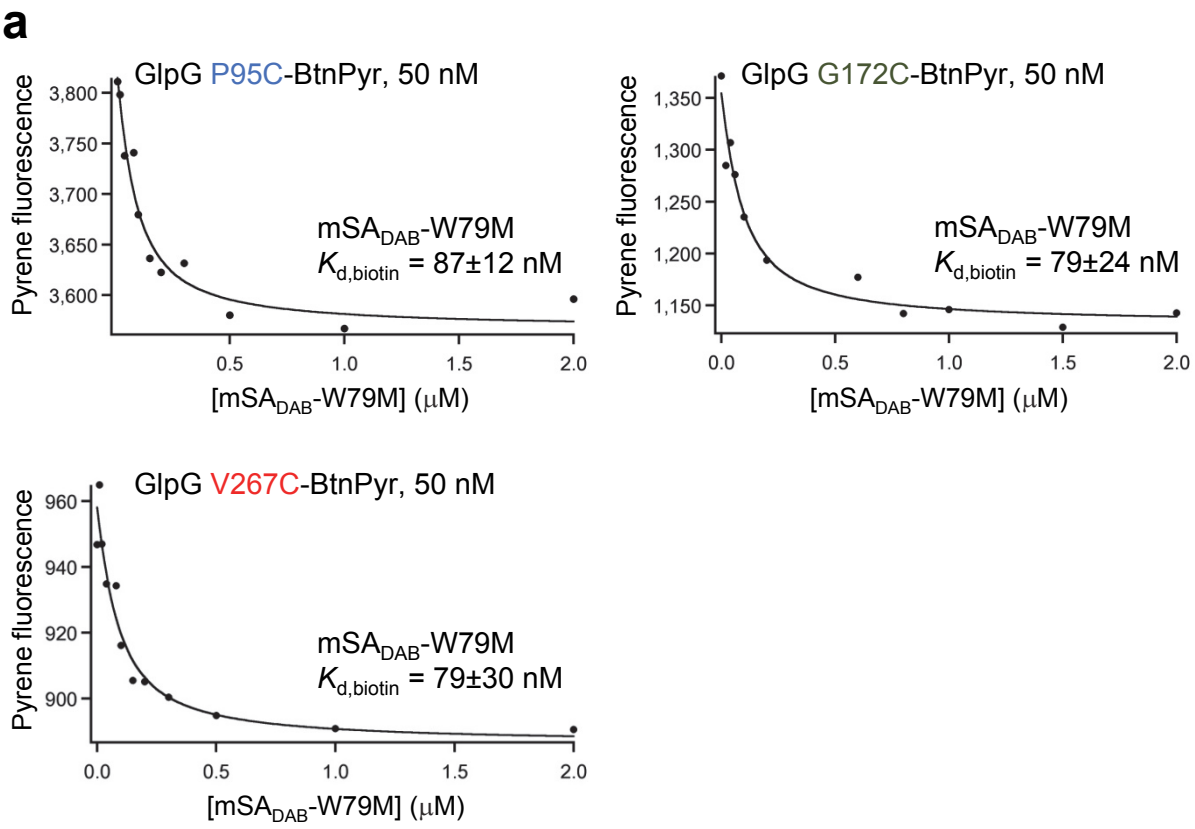

Supplementary Figure 3 | Determination of biotin affinity ($K_{d,biotin}$) of mSA variants by FRET. (a) Determination of $K_{d,biotin}$ for a weaker binding variant mSA-W79M labeled with a nonfluorescent quencher DABCYL (mSA$_{DAB}$-W79M). From these direct binding measurements, $K_{d,biotin}$'s for mSA$_{DAB}$ were similar for the biotin labels at three sites. See Online Methods for detailed procedures and fitting equation (**equation (5)**).

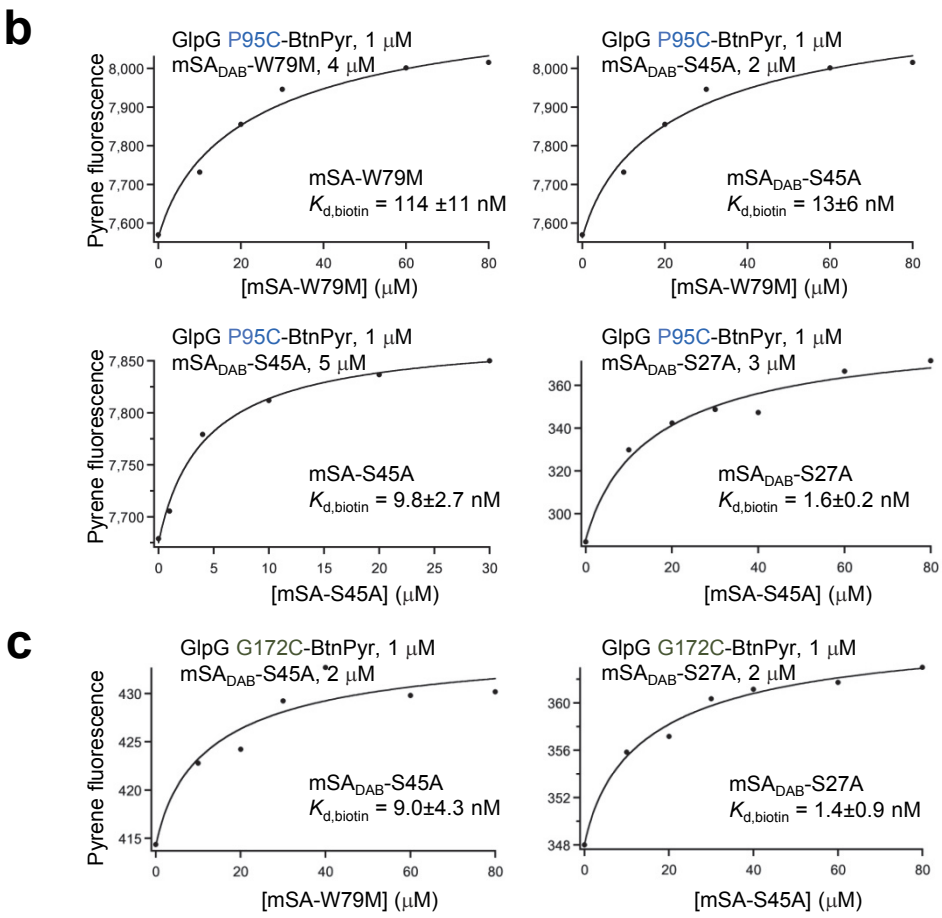

(Continued) Supplementary Figure 3 | Determination of biotin affinity ($K_{d,biotin}$) of mSA variants by FRET. (b) Determination of $K_{d,biotin}$ of high-affinity variants mSA$_{DAB}$-S45A and mSA$_{DAB}$-S27A with DABCYL label for P95C-BtnPyr site on GlpG by competition assay using FRET-based dequenching. **Top left:** determination of $K_{d,biotin}$ of mSA-W79M without DABCYL label using mSA$_{DAB}$-W79M with known $K_{d,biotin}$ obtained in **Supplementary Fig. 3a**. **Top right:** determination of $K_{d,biotin}$ of mSA$_{DAB}$-S45A using mSA-W79M with known $K_{d,biotin}$ obtained from the preceding plot. **Bottom left:** determination of $K_{d,biotin}$ of mSA-S45A using mSA$_{DAB}$-S45A with known $K_{d,biotin}$ obtained from the preceding plot. **Bottom right:** determination of $K_{d,biotin}$ of mSA$_{DAB}$-S27A using mSA-S45A with known $K_{d,biotin}$ obtained from the preceding plot. (**c**) Determination of $K_{d,biotin}$ of high-affinity variants mSA$_{DAB}$-S45A and S27A for G172C-BtnPyr site on GlpG using the same assay. **Left:** determination of $K_{d,biotin}$ of mSA$_{DAB}$-S45A using mSA-W79M with known $K_{d,biotin}$ obtained from **Supplementary Fig. 3a**. **Right:** determination of $K_{d,biotin}$ of mSA$_{DAB}$-S27A using mSA-S45A with known $K_{d,biotin}$ obtained from the preceding plot. Errors denote mean ± s. d. from the fitting. See Online Methods for detailed procedures and fitting equation (**equation (6)**)

d

X_{SDS}	mSA_{DAB}-W79M $K_{d,biotin}$ (nM)	mSA_{DAB}-S45A $K_{d,biotin}$ (nM)	mSA_{DAB}-S27A $K_{d,biotin}$ (nM)
0	79 ± 24	9.0 ± 4.3	1.4 ± 0.9
0.1	99 ± 27	5.5 ± 2.1	0.3 ± 0.1
0.2	100 ± 78	4.3 ± 2.7	0.4 ± 0.1
0.3	180 ± 50	5.8 ± 3.0	
0.4	260 ± 100	2.9 ± 0.6	
0.5	270 ± 70	5.8 ± 2.1	
0.6	560 ± 210	3.9 ± 2.0	

(Continued) Supplementary Figure 3 | Determination of biotin affinity ($K_{d,biotin}$) of mSA variants by FRET. (d) Summary of $K_{d,biotin}$'s for mSA_{DAB}-W79M determined by direct binding assays, and mSA_{DAB}-S45A and mSA_{DAB}-S27A determined by FRET-based competition assays in various mole fractions of SDS (X_{SDS}). All experiments were done using GlpG G172C-BtnPyr variant in 5 mM DDM, 20 mM Na_2HPO_4 (pH 7.5), 200 mM NaCl, 0.25 mM TCEP solution. Error bars denote mean ± s. d. from fitting.

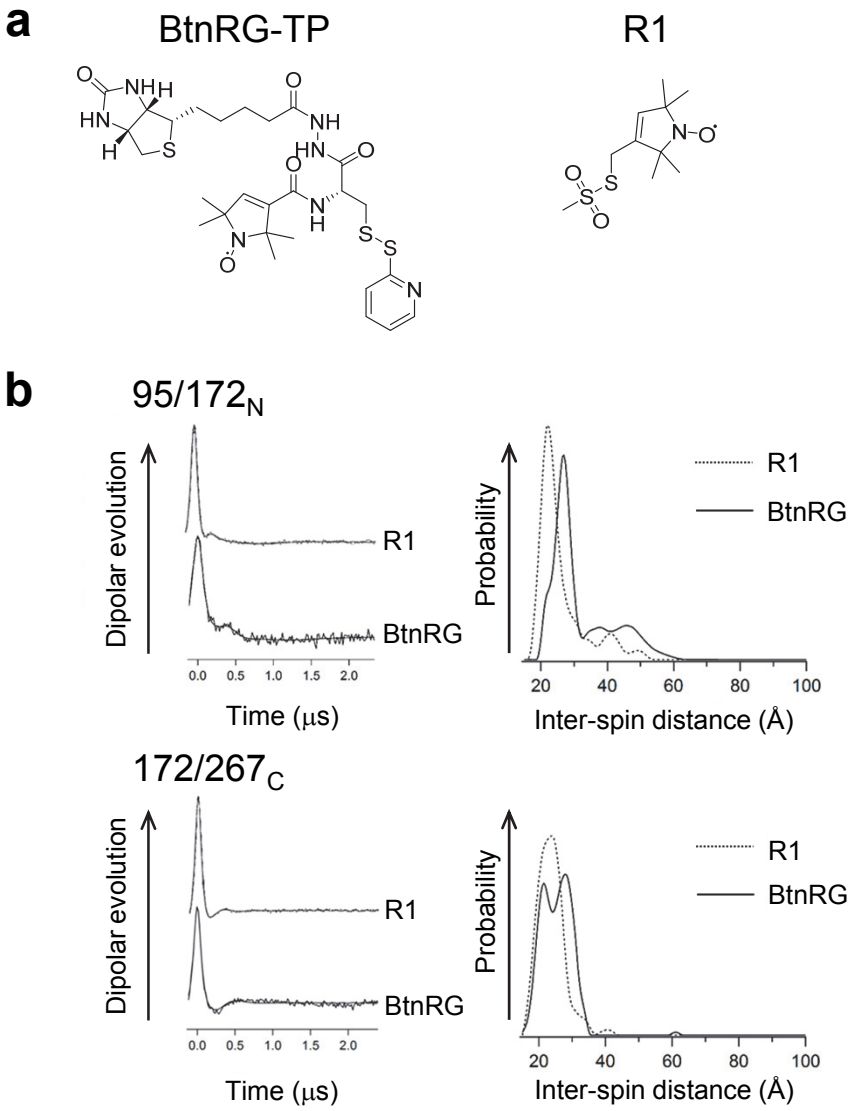

Supplementary Figure 4│ **Comparison of BtnRG to standard R1 spin label. (a)** Structures of BtnRG-TP and R1 spin labels. **(b)** Background-subtracted time-domain dipolar evolution data (**left**) and inter-spin distance distributions (**right**) comparing BtnRG- and R1-labeled double-cysteine variants in their native states.

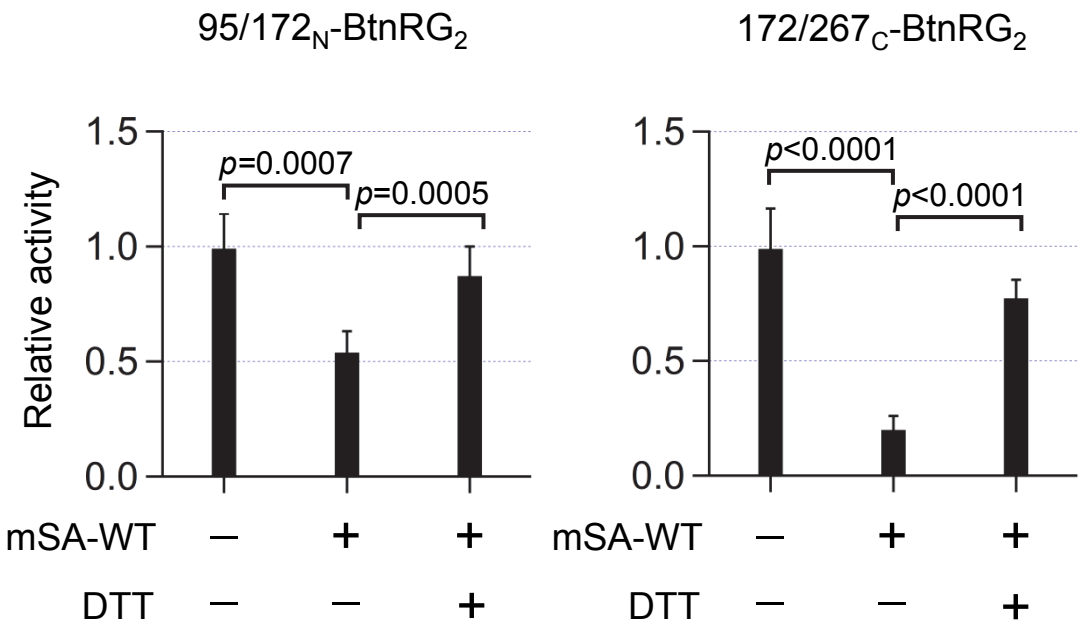

Supplementary Figure 5| **Characterization of activity and reversibility of GlpG labeled with paramagnetic BtnRG for steric trapping and DEER measurements.** Activity of GlpG was measured from the cleavage rate of NBD-labeled SN-LacYTM2 as described in **Supplementary Fig. 1**. Saturated binding of mSA-WT to each double-cysteine variant labeled with BtnRG led to an inactivation of GlpG. Folding reversibility was tested by addition of 4 mM of dithiothreitol (DTT) followed by incubation for 4 h at room temperature. DTT induced the cleavage of the disulfide linkage between cysteine on the protein and BtnRG label with bound mSA, which then released the steric restraints by two mSA molecules to allow for refolding. The activity levels were normalized relative to that of wild-type GlpG. Error bars denote mean ± s. d. (n=5 for the data without mSA and n=3 for the data with mSA). All *p*-values from Student's *t*-test were lower than 0.05, the threshold confidence level, indicating that the activity differences for unfolded and refolded states were statistically significant.

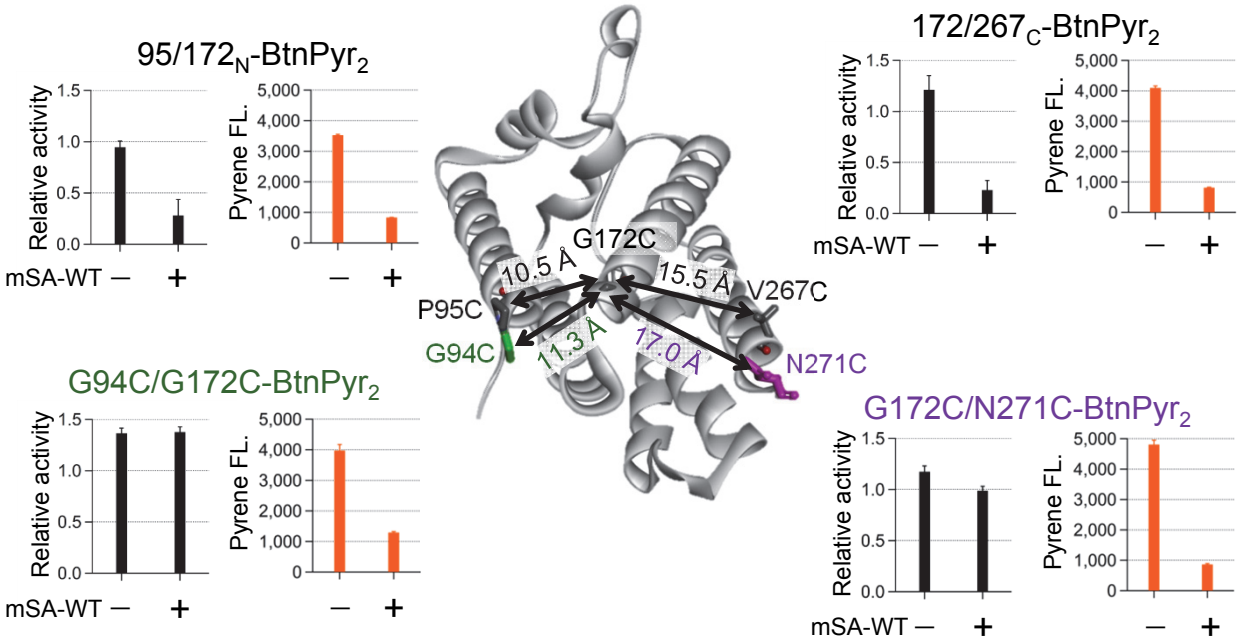

Supplementary Figure 6 | Coexistence of two monovalent streptavidin molecules within a close distance. For double-biotin variants 95/172$_N$-BtnPyr$_2$ and 172/267$_C$-BtnPyr$_2$, which were effective in steric trapping, addition of excess quencher-labeled mSA$_{DAB}$-WT induced substantial inactivation which indicated unfolding (black bars in top panels) and large quenching of pyrene fluorescence which indicated saturated binding (red bars in top panels). Two double cysteine mutants G94C/G172C and G172C/N271C whose C_α-C_α distances (11.3 Å and 17.0 Å, respectively) were similar to those of 95/172$_N$ and 172/267$_C$ (10.5 Å and 15.5 Å, respectively). However, for these variants labeled with BtnPyr, addition of excess mSA$_{DAB}$-WT retained the native activity level which indicated no unfolding (black bars in lower panels) but induced large fluorescence quenching which indicated saturated binding (red bars in lower panels). Error bars denote mean ± s. d. (n=3).

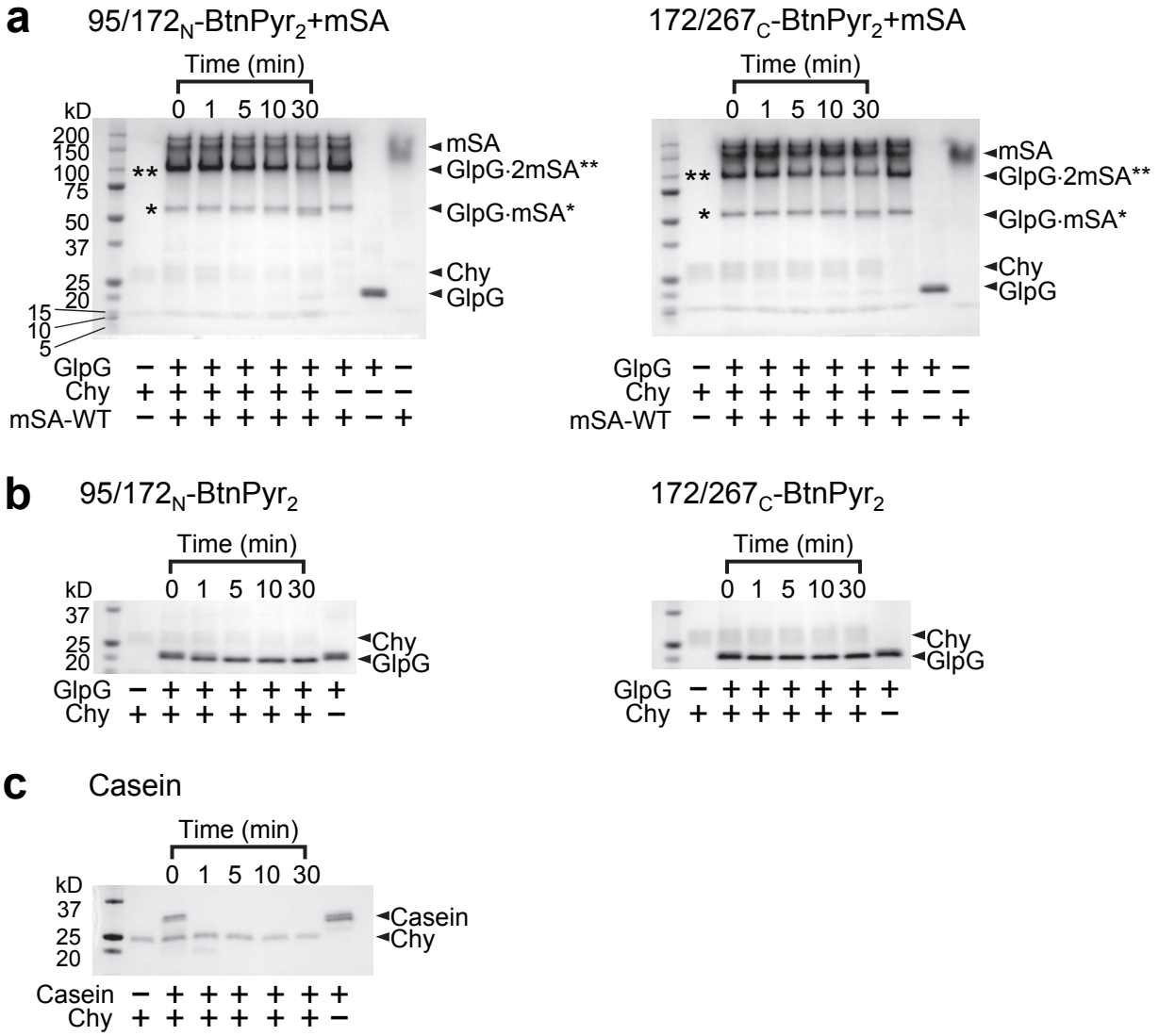

Supplementary Figure 7| Probing the flexibility of the steric-trapped unfolded state of GlpG using proteolysis and SDS-PAGE. (a) Time-dependent proteolysis of the steric-trapped unfolded states (GlpG·2mSA, marked with **) of 95/172$_N$-BtnPyr$_2$ (left) and 172/267$_C$-BtnPyr$_2$ (right) by chymotrypsin (Chy). **(b)** Proteolysis of native double-biotin variants in the absence of mSA. Those samples exhibited only partial digestion of the terminal flexible regions (Wang *et al.* **2006** *Nature* 444, 179-180). **(c)** Proteolysis of casein as a control of protein substrate lacking significant ordered secondary structures. Detailed procedures are described in Online Methods

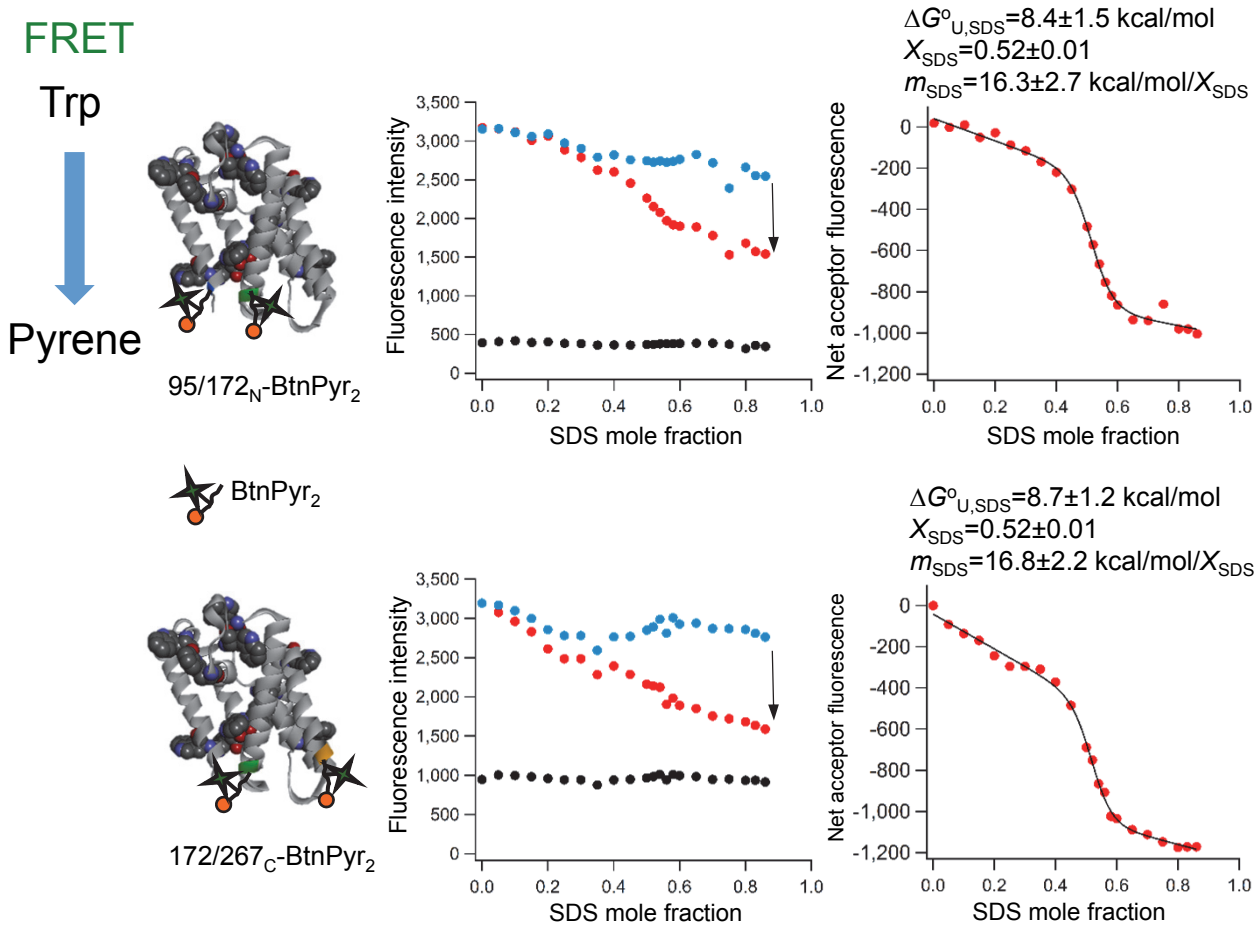

Supplementary Figure 8 | Denaturation curves induced by SDS for double-cysteine GlpG variants labeled with BtnPyr. (**Left column**) Due to the spectral overlap between tryptophan fluorescence and pyrene absorption, Förster resonance energy transfer (FRET) occurred between intrinsic tryptophan residues of GlpG (donor, spheres) and pyrene in the BtnPyr label (acceptor). (**Middle column**) In the native state (SDS mole fraction=[SDS]/([SDS]+[DDM])=0), FRET led to large suppression of tryptophan fluorescence (black dots, λ_{Ex}=280 nm and λ_{Em}=330 nm) and enhancement of pyrene fluorescence (red dots, λ_{Ex}=295 nm and λ_{Em}=385 nm). Here λ_{Ex}=295 nm was chosen to selectively excite tryptophan. As SDS induced unfolding of GlpG, pyrene (acceptor) fluorescence was suppressed by the inefficient FRET from tryptophan (donor) (traces of red dots). We also took into account the change of pyrene fluorescence depending on SDS mole fraction (blue dots, λ_{Ex}=345 nm and λ_{Em}=418 nm). Here λ_{Ex}=345 nm was chosen to selectively excite pyrene. λ_{Em}=418 nm was chosen to match with pyrene fluorescence by FRET at zero SDS mole fraction. (**Right column**) By taking the difference between pyrene fluorescence not affected by FRET (blue dots) and pyrene fluorescence affected by FRET (red dots), an SDS-induced unfolding curve was obtained. The unfolding curves were fitted to a two-state Santoro-Bolen equation (Online Methods**, equations (7)** and **(8)**) to determine the free energy of unfolding ($\Delta G^{\circ}_{U,SDS}$), transition midpoint ($X_{SDS,1/2}$) and slope of the transition (m_{SDS}-value).

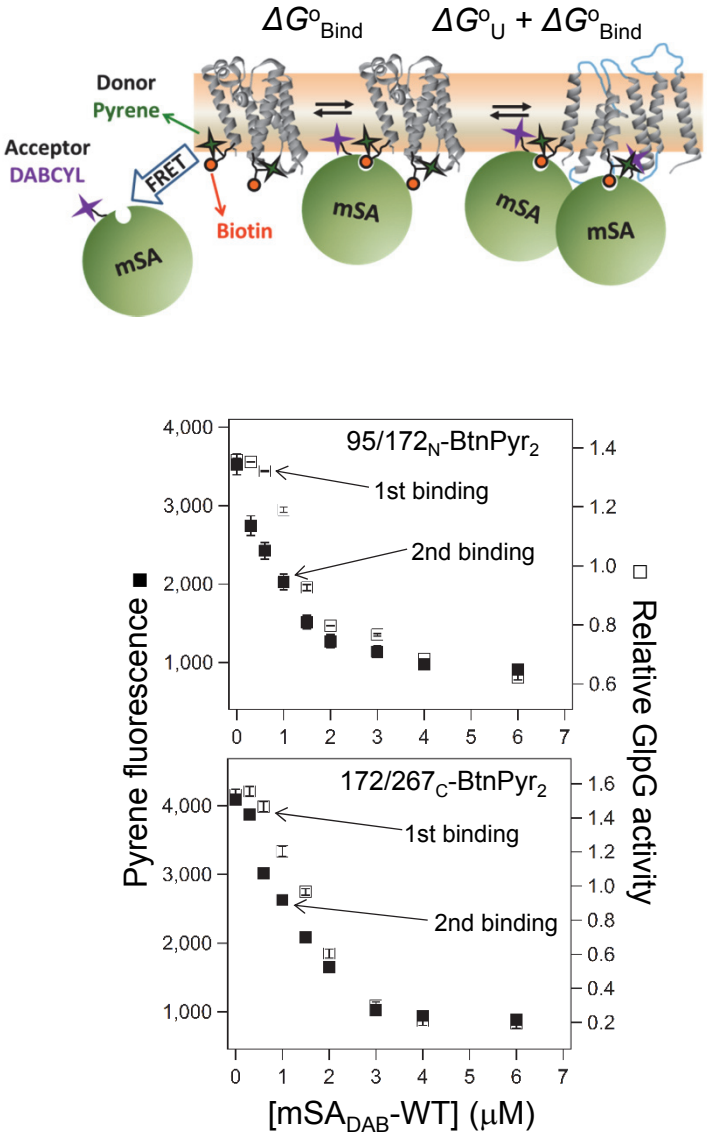

Supplementary Figure 9 | The second binding phase is coupled to the unfolding monitored by activity. Inactivation of GlpG variants $95/172_N$-$BtnPyr_2$ and $172/267_C$-$BtnPyr_2$ (1 μM) at an increasing concentration of quencher (DABCYL)-labeled wild-type monovalent streptavidin (mSA_{DAB}–WT). In the first binding phase ([mSA_{DAB}-WT] <1 μM), pyrene fluorescence decreased while activity remained the same. As the concentration of mSA increased higher than the concentration of GlpG ([mSA_{DAB}-WT]>1 μM), binding of a second mSA coincided with the decrease of activity, indicating the unfolding-binding coupling. Activity of GlpG is relative to that of wild-type GlpG. Error bars denote mean ± s. d. from 4 independent measurements (pyrene fluorescence) or the fitting (activity).

a *Step 1*: analyze tertiary interactions using side-chain contact map

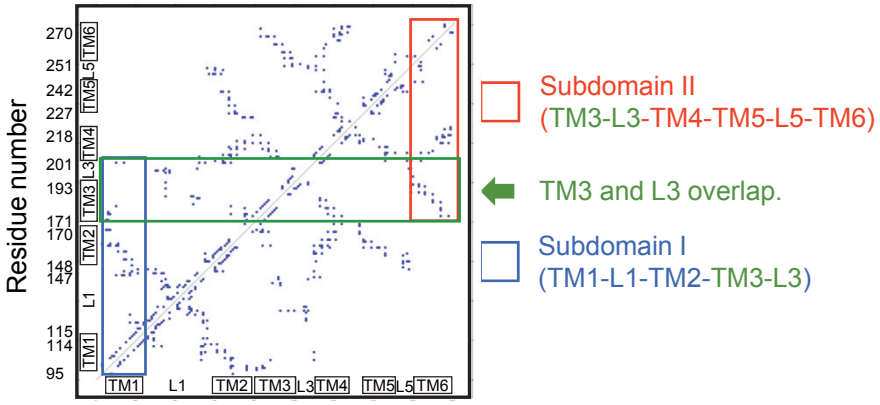

Step 2: define subdomain II using experimental *m*-values and predicted Δ*ASA*s

TM1~TM6 unfolding

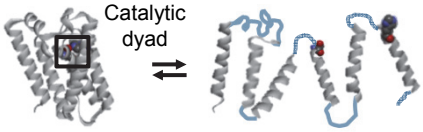

Δ*ASA*=11,635.1 Å^2

m = 16.3 ±3.4 kcal/mol/X_{SDS}
(global unfolding, SDS denaturation)

$L3_{199}$-TM4-TM5-L5-TM6 unfolding

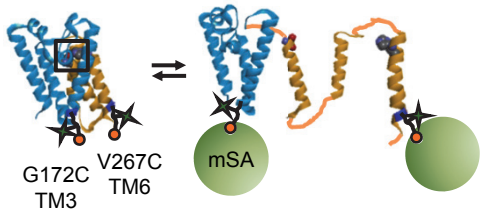

Δ*ASA*=6,309.7 Å^2

m = 8.4 ±1.1 kcal/mol/X_{SDS}
(subglobal unfolding, steric trapping)

$$Ratio_{m\text{-value}} = \frac{m_{\text{subglobal unfolding}}}{m_{\text{global unfolding}}} = 0.53 \pm 0.13 \qquad Ratio_{\Delta ASA} = \frac{\Delta ASA_{L3_{199}\sim TM6\ \text{unfolding}}}{\Delta ASA_{TM1\sim TM6\ \text{unfolding}}} = 0.54$$

Supplementary Figure 10 | Strategy of subdomain dissection for the cooperativity analysis. **(a)** *Step 1*: Analysis of side-chain contacts in the structure of GlpG (PDB: 3B45, 1.9 Å resolution) within 5 Å interatomic distances (Discovery Studio program, Accelrys). TM1 to which a biotin label is conjugated in GlpG 95/172$_N$-BtnPyr$_2$ makes contacts with L1, TM2, TM3 and L3. TM6 to which a biotin label is conjugated in GlpG 172/267$_C$-BtnPyr$_2$ makes contacts with TM3, L3, TM4, TM5, L5 and TM6. Thus, TM3 and L3 overlap between the two contacting regions. *Step 2*: To precisely define whether overlapping TM3 and L3 belong to subdomain I or II, we used the facts that the C-terminal region undergoes subglobal unfolding and *m*-value is correlated with the exposed accessible surface area upon unfolding (Δ*ASA*, see the detailed scheme for calculating Δ*ASA* below). The ratio of the *m-value* for subglobal unfolding identified with the C-terminal biotin pair 172/267$_C$-BtnPyr$_2$ to that for global unfolding from SDS denaturation was = 0.53 ±0.13 (**Fig. 5**). We calculated the predicted Δ*ASA* upon successive unfolding of the C-terminal TM helices until the ratio of Δ*ASA* for the C-terminal unfolding to Δ*ASA* for global unfolding approximately reached the ratio of *m*-values (0.53±0.13). It was achieved when $L3_{199}$-TM4-TM5-L5-TM6 was unfolded while the structure of TM1-L1-TM2-TM3 remained intact (Δ*ASA* ratio=0.54). Thus, subdomain I was defined as TM1-L1-TM2-TM3-$L3_{198}$ and the subdomain II was defined as $L3_{199}$-TM4-TM5-L5-TM6.

b

Predicted ΔASA for global unfolding

AA range	Structural elements	*ASA* (Å^2)
91-270	Native GlpG	9,310.6
Unraveled secondary-structural fragments		
91-114	TM1	2,508.2
115-128	L1 Helix 1	1,773.6
129-134	L1 Helix 2	887.6
135-147	L1 Helix 3	1,811.8
148-170	TM2	2,619.8
171-193	TM3	2,305.6
194-200	L3	1,006.1
201-218	TM4	1,955.2
219-226	L4	1,111.2
227-242	TM5	1,880.9
243-250	L5	1,175.8
251-270	TM6	1,909.9
	Sum of *ASA* in the unfolded state	20,945.7
Exposed area upon unfolding (ΔASA)		11,635.1

Predicted ΔASA for subglobal unfolding

AA range	Structural elements	*ASA* (Å^2)
91-270	Native GlpG	9,310.6
Folded fragment		
91-198	TM1-L1-TM2-TM3-$L3_{198}$	7,212.4
Unraveled secondary-structural fragments		
199-200	$L3_{199-200}$	374.9
201-218	TM4	1,955.2
219-226	L4	1,111.2
227-242	TM5	1,880.9
243-250	L5	1,175.8
251-270	TM6	1,909.9
	Sum of *ASA* in the unfolded state	8,407.9
Exposed area upon unfolding (ΔASA)		6,309.7

(Continued) Supplementary Figure 10 | Strategy of subdomain dissection for the cooperativity analysis. (b) Calculation of the predicted ΔASA upon unfolding using the high-resolution structure of GlpG (PDB: 3B45, 1.9 Å resolution) and a 1.4 Å-radius probe (Lee & Richards **1971** *J Mol Biol* 55, 379–400). In the calculation, we assumed that the native secondary structure was kept in individual unraveled TM helices and major loops (L1, L3, L4 and L5). This assumption was supported by the fact that the far-UV circular dichroism spectrum of the SDS-unfolded state was identical to that of native GlpG, indicating that the secondary structural content was maintained in the unfolded state (Baker & Urban **2012** *Nat. Chem. Biol.* 8, 759). For the globally-unfolded state achieved by SDS denaturation, its *ASA* was calculated as the sum of the *ASA*'s of individual secondary structural fragments whose PDB files were generated from the native GlpG structure. Thus, the $\Delta ASA_{\text{global unfolding}} = ASA_{\text{sum of ASAs in the unfolded state}} - ASA_{\text{native GlpG}}$. For the subglobally-unfolded state that was obtained by steric trapping using the C-terminal biotin pair $172/267_C$-$BtnPyr_2$, we assumed that the C-terminal TM helices and loops were unraveled and the native tertiary structure was maintained in the remaining N-terminal region. Thus, $\Delta ASA_{\text{subglobal unfolding}} = [ASA_{\text{folded N-term. fragment}} + ASA_{\text{sum of ASAs in the unfolded C-term.}}] - ASA_{\text{native GlpG}}$.

c

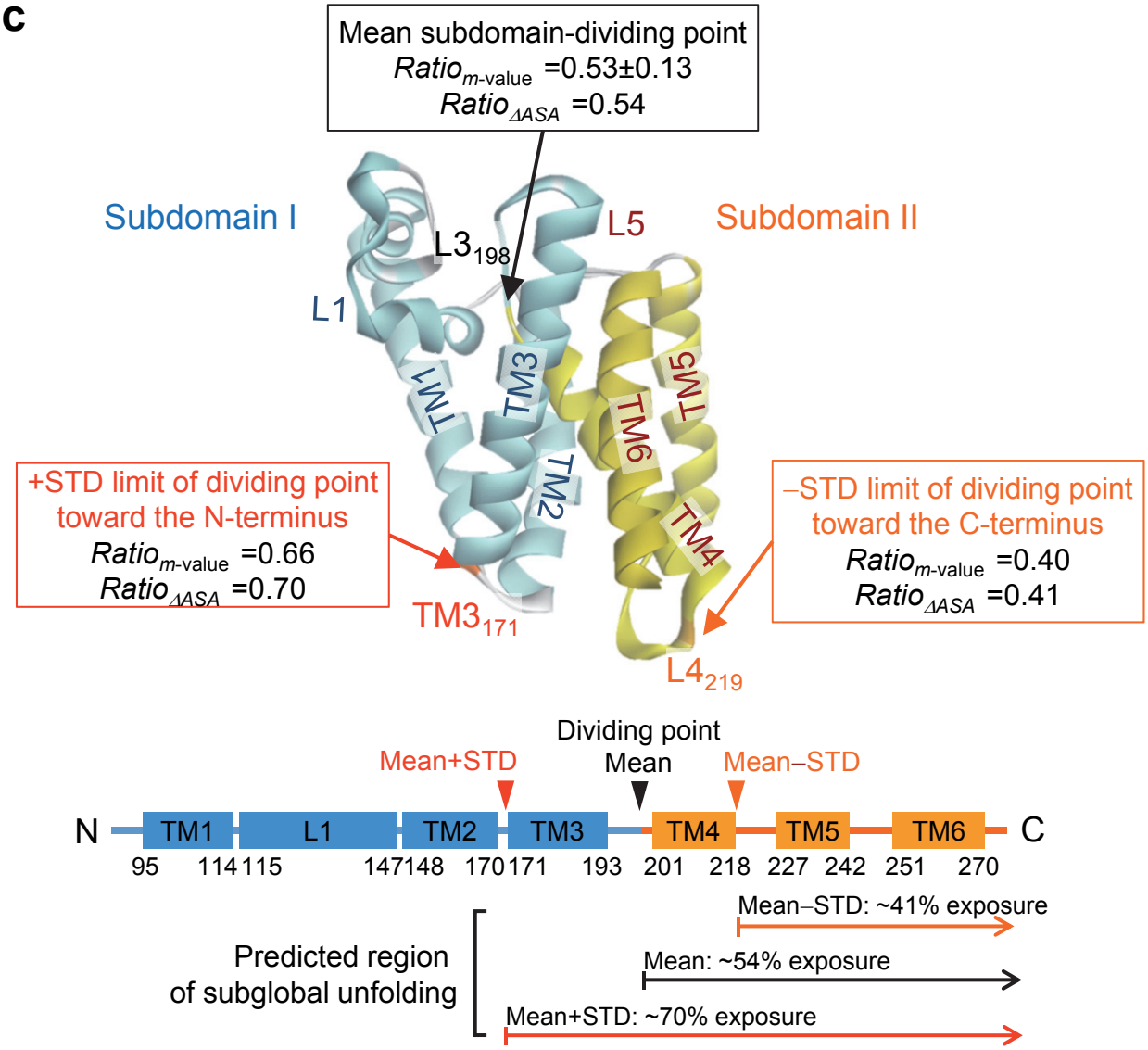

(Continued) Supplementary Figure 10 | Strategy of subdomain dissection for the cooperativity analysis. (c) Estimated uncertainty of the subdomain-dividing point (residue 198 in the L3 loop) mapped onto the structure (**top**) and the amino acid sequence (**bottom**). Due to the error in $Ratio_{m\text{-value}}$ (0.53±0.13), which was calculated from the error in the *m*-value for subglobal unfolding ($m_{\text{subglobal unfolding}}$= 8.4±1.2) and the error in the *m*-value for SDS denaturation ($m_{\text{SDS unfolding}}$= 16.3±3.4), straightforward determination of the subdomain-dividing point was difficult. Therefore, we defined its uncertainty using the standard deviation (STD, ±0.13) of $Ratio_{m\text{-value}}$ ("Mean" at 0.53). In the upper STD limit ("Mean+STD", $Ratio_{m\text{-value}}$=0.66), the best-matching $Ratio_{\Delta ASA}$ (~0.70) was obtained when subglobal unfolding occurred from residue 171 to the C-terminus. On the other hand, in the lower limit ("Mean–STD", $Ratio_{m\text{-value}}$ =0.40), the best-matching $Ratio_{\Delta ASA}$ (~0.41) was obtained when subglobal unfolding occurred from residue 219 to the C-terminus.

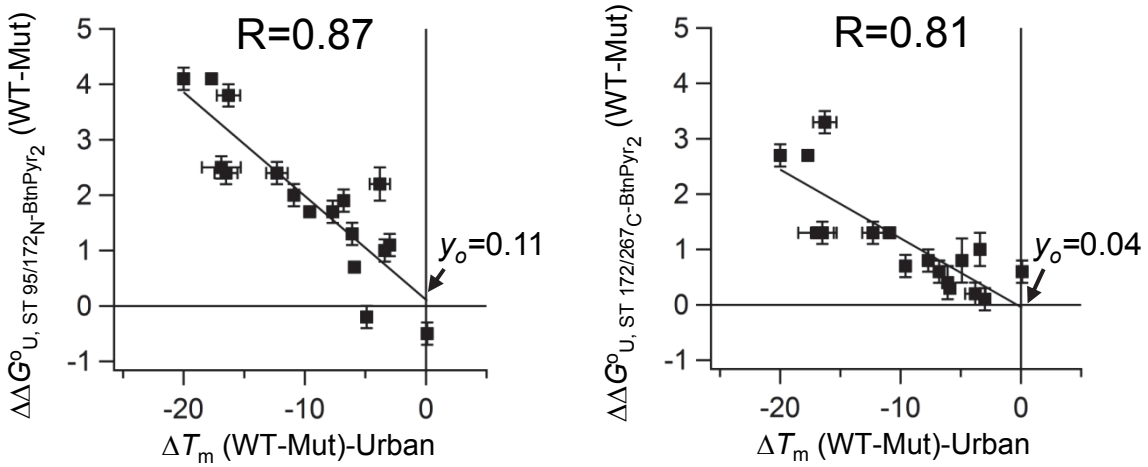

Supplementary Figure 11 | Comparisons of the stabilities obtained by steric trapping to those obtained by thermal denaturation. The correlation between the destabilization energies by mutation from steric trapping ($\Delta\Delta G^o_{U,ST}$ (WT-Mut) = $\Delta G^o_{U,ST}$ (WT) – $\Delta G^o_{U,ST}$ (Mut)) and the changes in melting temperature from thermal denaturation (ΔT_m (WT-Mut)-Urban = T_m (WT) – T_m (Mut)) (Baker and Urban **2012** *Nat. Chem. Biol.* 8, 759) was tested. ΔT_m (WT-Mut)-Urban was compared to $\Delta\Delta G^o_{U,ST}$ (WT-Mut) obtained in the backgrounds of both $95/172_N$-$BtnPyr_2$ and $172/267_C$-$BtnPyr_2$ for 17 common mutations. Error bars for $\Delta\Delta G^o_{U,ST}$ (WT-Mut) denote the propagated errors of individual errors in $\Delta G^o_{U,ST}$ values (± s. d. from fitting). Error bars for ΔT_m were taken from the work by Baker and Urban.

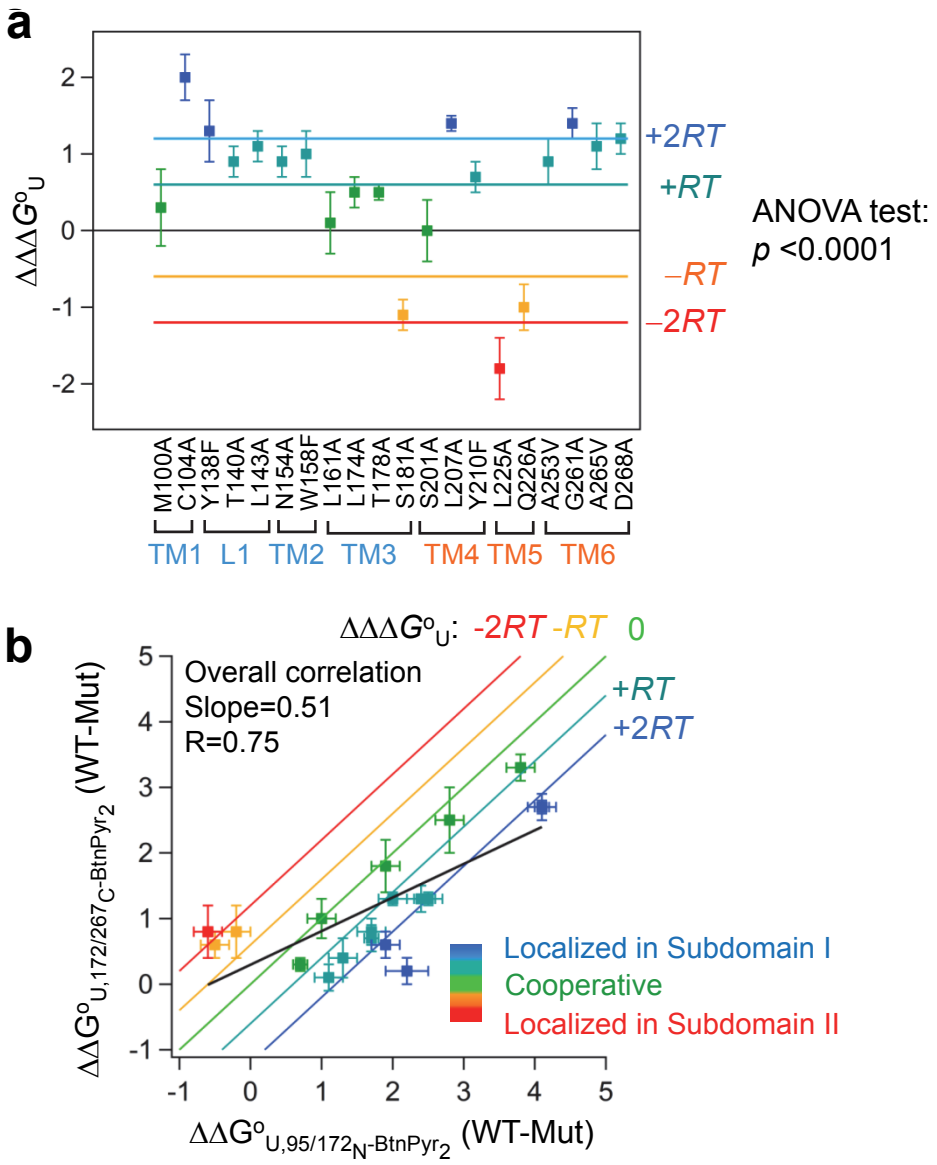

Supplementary Figure 12 | Distribution of $\Delta\Delta\Delta G^{o}_{U}$ and $\Delta\Delta G^{o}_{U}$ values used for the assignment of the cooperativity profile (a) Distribution of $\Delta\Delta\Delta G^{o}_{U}$ values. Horizontal lines indicate the multiples of thermal fluctuation energy *RT* (0.6 kcal/mol at 25 °C), the cut-off values used for the assignment of the cooperativity profile. An ANOVA test of the five sets of $\Delta\Delta\Delta G^{o}_{U}$ values yielded p<0.0001, which indicates that the difference of these sets was statistically significant. **(b)** Correlation between $\Delta\Delta G^{o}_{U}$(WT-Mut) values in the background of the two double-biotin variants $95/172_{N}$-$BtnPyr_2$ and $172/267_{C}$-$BtnPyr_2$. Colored diagonal lines correspond to the cut-off $\Delta\Delta\Delta G^{o}_{U}$ values. Black line indicates the overall correlation between the two sets of $\Delta\Delta G^{o}_{U}$ values. In both **(a)** and **(b)**, symbols were color-coded according to their corresponding cooperativity profile: green (cooperative), teal (moderately localized in subdomain I), blue (highly localized in subdomain I), orange (moderately localized in subdomain II) and red (highly localized in subdomain II). The error bars for $\Delta\Delta\Delta G^{o}$ and $\Delta\Delta G^{o}_{U,ST}$ (WT-Mut) denote the propagated errors of individual errors in $\Delta G^{o}_{U,ST}$ values (± s. d. from fitting).

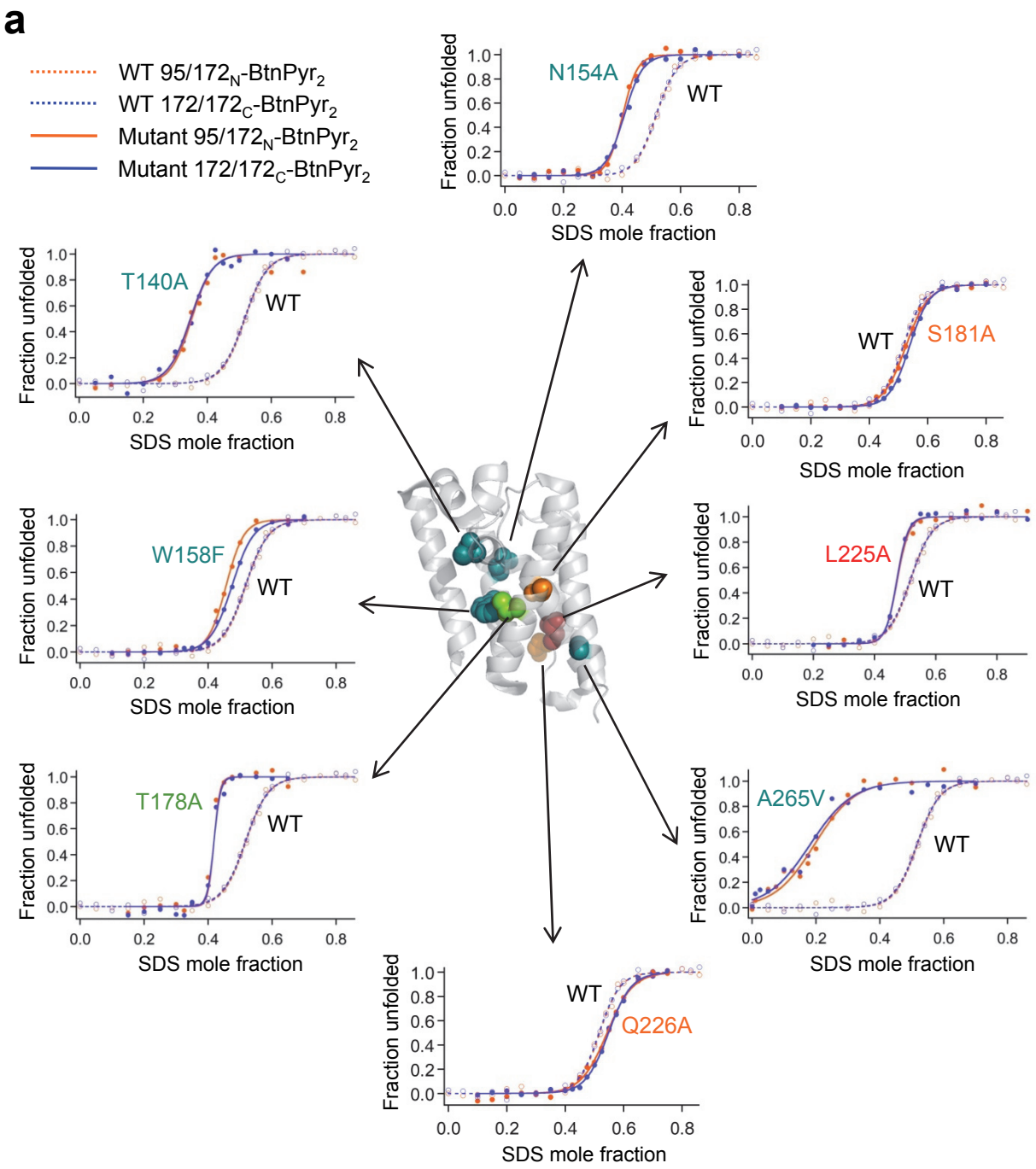

Supplementary Figure 13 | SDS denaturation of mutants. (a) Mutations of 8 residues with various cooperativity profiles measured by steric trapping were chosen. $\Delta G^{\circ}_{U,SDS}$ was obtained for both 95/172$_N$-BtnPyr$_2$ (blue filled circles) and 172/267$_C$-BtnPyr$_2$ (red filled circles) backgrounds. "WT" refers to 95/172$_N$-BtnPyr$_2$ (blue open circles) and 172/267$_C$-BtnPyr$_2$ (red open circles) with no other mutation. Mutated residues were color-coded according to their cooperativity profile (**Fig. 6b**). See Online Methods for detailed procedures.

b

Mutation	Background	$\Delta G^{\circ}_{U,SDS}$ (kcal/mol)	$X_{SDS,\ 1/2}$	m_{SDS} (kcal/mol/X_{SDS})
Wild type	$95/172_N$-$BtnPyr_2$	8.4 ± 1.5	0.52 ± 0.01	16.3 ± 2.7
	$172/267_C$-$BtnPyr_2$	8.7 ± 1.2	0.52 ± 0.01	16.8 ± 2.2
T140A	$95/172_N$-$BtnPyr_2$	5.8 ± 1.8	0.35 ± 0.01	16.7 ± 4.2
	$172/267_C$-$BtnPyr_2$	3.8 ± 1.7	0.31 ± 0.02	12.5 ± 3.7
N154A	$95/172_N$-$BtnPyr_2$	7.7 ± 1.2	0.41 ± 0.01	18.7 ± 2.4
	$172/267_C$-$BtnPyr_2$	9.4 ± 1.4	0.40 ± 0.01	23.6 ± 2.8
W158F	$95/172_N$-$BtnPyr_2$	8.7 ± 1.0	0.48 ± 0.01	18.1 ± 2.0
	$172/267_C$-$BtnPyr_2$	9.8 ± 1.4	0.46 ± 0.01	21.3 ± 3.0
T178A	$95/172_N$-$BtnPyr_2$	24.6 ± 5.0	0.41 ± 0.02	60.0 ± 9.3
	$172/267_C$-$BtnPyr_2$	26.3 ± 3.4	0.41 ± 0.01	64.2 ± 6.9
S181A	$95/172_N$-$BtnPyr_2$	9.3 ± 0.7	0.54 ± 0.01	17.3 ± 1.1
	$172/267_C$-$BtnPyr_2$	8.2 ± 0.6	0.53 ± 0.01	15.5 ± 0.9
L225A	$95/172_N$-$BtnPyr_2$	15.3 ± 3.6	0.47 ± 0.01	32.5 ± 6.1
	$172/267_C$-$BtnPyr_2$	17.5 ± 2.4	0.47 ± 0.01	37.3 ± 4.8
Q226A	$95/172_N$-$BtnPyr_2$	8.4 ± 0.9	0.55 ± 0.01	15.2 ± 1.3
	$172/267_C$-$BtnPyr_2$	7.4 ± 1.0	0.55 ± 0.01	13.4 ± 1.5
A265V	$95/172_N$-$BtnPyr_2$	1.8 ± 2.2	0.20 ± 0.01	8.9 ± 0.9
	$172/267_C$-$BtnPyr_2$	1.7 ± 2.3	0.18 ± 0.01	9.4 ±1.0

(Continued) Supplementary Figure 13 | SDS denaturation of mutants. (b) Table displaying $\Delta G^{\circ}_{U,SDS}$, $X_{SDS,½}$, and m_{SDS} determined for each mutation in $95/172_N$-$BtnPyr_2$ and $172/267_C$-$BtnPyr_2$ backgrounds. For each mutation, there was no significant difference in the stability measured by SDS denaturation between the two backgrounds. The errors denote mean ± s. d from the fitting of data in **Supplementary Fig. 13a**.

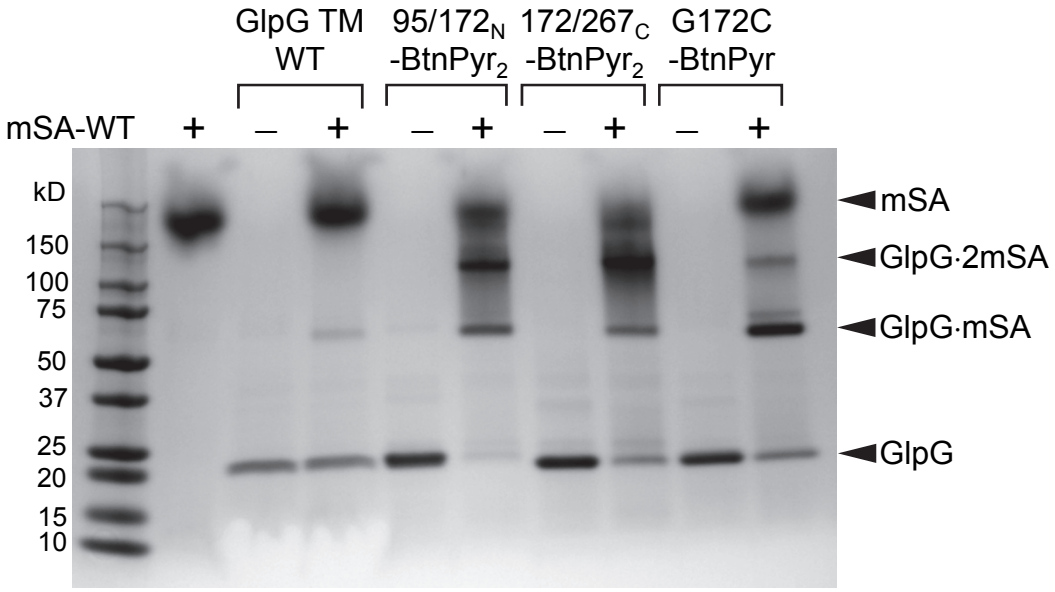

Supplementary Figure 14| **Determination of labeling efficiency using SDS-PAGE gel shift assay.** Detailed procedures is described in Online Methods**.** For wild-type (WT) GlpG possessing a native buried cysteine residue C104, after labeling reaction, there was a minor GlpG·mSA band demonstrating that labeling of this residue or nonspecific labeling was negligible. For $95/172_N$ (labeling efficiency≈1.5) and $172/267_C$ (labeling efficiency≈1.6), major GlpG·2mSA bands existed with minor unlabeled and GlpG·mSA bands. For single-cysteine variant G172C, a strong GlpG·mSA band appeared with minor unlabeled and GlpG·2mSA (over-labeled) bands. mSA-WT (52 kD, the second lane) migrated as a larger molecular species (>150 kD) probably due to an abnormal number of SDS molecules bound to a tetrameric mSA molecule.

Supplementary Notes: Compound synthesis and characterization

1) BtnPyr-IA

a. Synthesis protocol for BtnPyr-IA

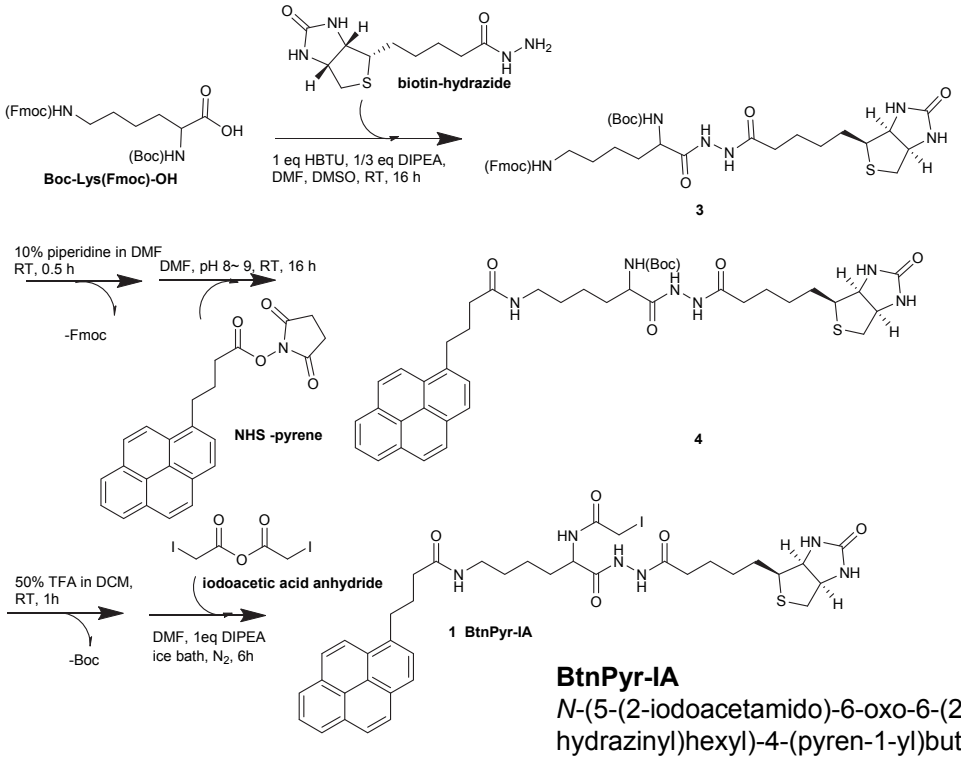

BtnPyr-IA
N-(5-(2-iodoacetamido)-6-oxo-6-(2-(+)-Biotin hydrazinyl)hexyl)-4-(pyren-1-yl)butanamide

Synthesis of fluorescent BtnPyr-IA. Boc-Lys(Fmoc)-OH (Chem-Impex International, 98.29% by HPLC) was used as a template. Iodoacetamide group, biotin and pyrene groups were conjugated to the template step by step. 362 mg (0.78 mmol) of Boc-Lys(Fmoc)-OH was activated by addition of 439 mg (1.16 mmol) of *O*-(Benzotriazol-1-yl)-*N,N,N′,N′*-tetramethyluronium hexafluorophosphate (HBTU) (Chem-Impex International, ≥99% by HPLC) and 50 μL (0.28 mmol) of *N,N*-Diisopropylethylamine (DIPEA) (Sigma, 99.5%) in 2 mL dimethyformamide (DMF) (Sigma, anhydrous, 99.8%). After incubation for 20 min, 100 mg (0.39 mmol) of biotin-hydrazide (Santa Cruz Biotechnology) dissolved in 1 mL of dimethyl sulfoxide (DMSO) (Avantor Performance Materials) was added dropwise and stirred at room temperature overnight. Then, excess diethyl ether (Sigma) was added to the reaction to make separated two layers. After removing the upper layper, ethyl acetate (Sigma) was added to the yellow lower layer to precipitate out **3**. The precipitation was washed several times with diethyl ether. Deprotection of Fmoc was performed with a 30-min incubation of **3** in 10% v/v piperidine (Sigma, ≥99.5%) in DMF followed by precipitation with diethyl ether. The yield at this point was ~50%. Then the product (Boc-Lys-biotin) was dissolved in 2 mL DMF and diethylamine (Sigma) solution (pH~8). After addition of 1.5 times molar excess of 1-Pyrenebutyric acid *N*-hydroxysuccinimide ester (NHS-pyrene) (Sigma, 95%), the mixture was stirred overnight at room temperature in dark. The following steps were carried out in dark. **4** was precipitated out with diethyl ether. Deprotection of Boc group was performed by incubation of **4** in 50% trifluoroacetic (TFA) acid (Sigma) in dichloromethane (DCM) (Sigma) for 30 min. After precipitation with diethyl ether, the product was dissolved in DMF. The solution was put in an ice bath and one equivalent of DIPEA and 1.5 times molar excess of iodoacetic acid anhydride (Sigma) dissolved in DMF were slowly added. The reaction mixture was protected with N_2 gas and incubated for 4 h. The final product **1** was precipitated out as light yellow powder with diethyl ether and analyzed by electron spray ionization (ESI) mass spectrometry (Xevo G2-S QTof, Waters). The exact mass of M+H is 825.2287 and the actual peak was at 825.2308 .Total yield was about 10%.

b. ESI-Mass analysis of BtnPyr-IA

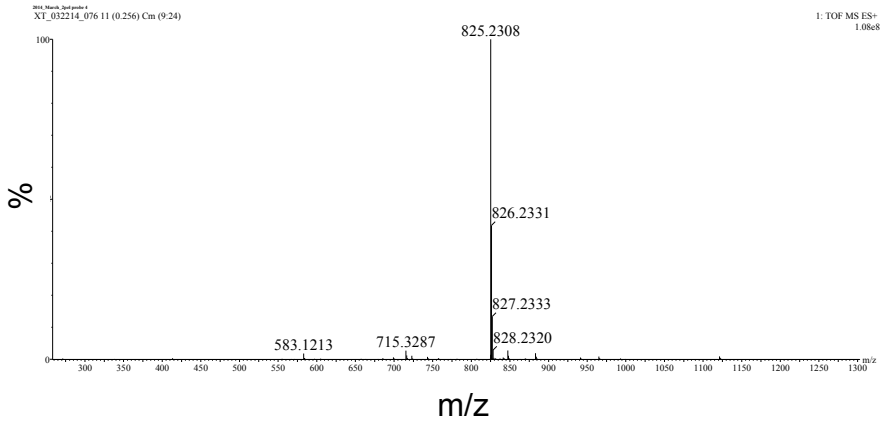

c. ^{1}H NMR analysis of BtnPyr-IA

^{1}H NMR (500 MHz, DMSO-d_6): δ 9.93 (s, 1H), 9.75 (s, 1H), 8.44 (d, *J* = 8.3 Hz, 1H), 8.36 (d, *J* = 9.3 Hz, 1H), 8.30 -8.16 (m, 4H), 8.16-8.07 (m, 2H), 8.04 (t, *J* = 7.6 Hz, 1H), 7.92 (d, *J* = 7.8 Hz, 1H), 7.78 (t, *J* = 5.5 Hz, 1H), 4.25 (dd, *J* = 12.9, 7.4 Hz, 2H), 4.12-4.03 (m, 1H), 3.66 (dd, *J* = 24.4, 9.7 Hz, 2H), 3.33-3.24 (m, 2H), 3.10-2.95 (m, 3H), 2.77 (dd, *J* = 12.4, 5.1 Hz, 1H), 2.53 (t, *J* = 12.7 Hz, 1H), 2.21 (t, *J* = 7.3 Hz, 2H), 2.07 (dd, *J* = 15.2, 7.3 Hz, 2H), 1.99 (dt, *J* = 15.1, 7.5 Hz, 2H), 1.70-1.17 (m, 13H).

d. ^{13}C NMR analysis of BtnPyr-IA

^{13}C NMR (126 MHz, DMSO-d_6) δ 172.10, 171.43, 170.71, 163.14, 137.01, 131.31, 130.86, 129.72, 128.58, 128.00, 127.89, 127.66, 126.93, 126.57, 125.38, 125.24, 124.66, 124.57, 123.95, 61.44, 59.59, 56.38, 55.82, 35.44, 34.21, 32.74, 29.69, 29.22, 28.92, 28.47, 28.32, 28.01, 25.86, 25.43, 22.69.

2) BtnRG-TP

a. Synthesis protocol for BtnRG-TP

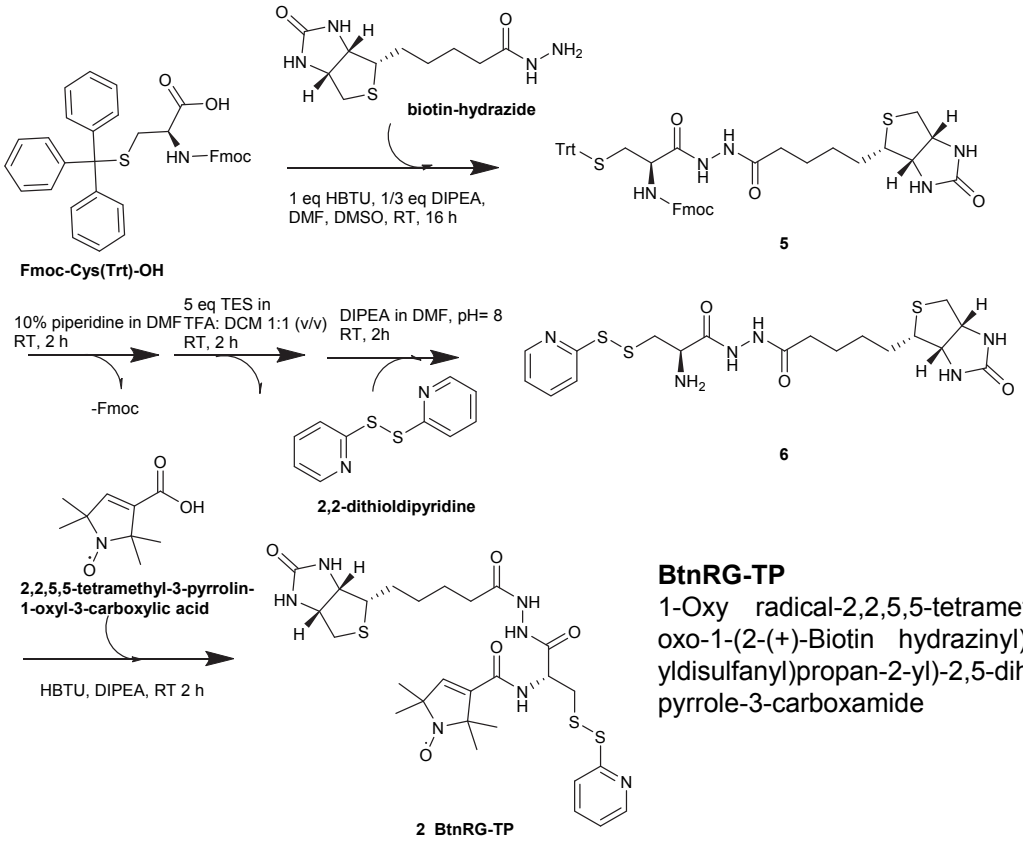

BtnRG-TP
1-Oxy radical-2,2,5,5-tetramethyl-*N*-((*R*)-1-oxo-1-(2-(+)-Biotin hydrazinyl)-3-(pyridin-2-yldisulfanyl)propan-2-yl)-2,5-dihydro-1*H*-pyrrole-3-carboxamide

Synthesis of paramagnetic BtnRG-TP. Fmoc-Cys(Trt)-OH (Chem-Impex International, ≥99% by HPLC) was used as a template. Iodoacetamide, biotin and spin label (2,2,5,5-Tetramethyl-3-pyrrolin-1-oxyl) groups were conjugated step by step. 340 mg (0.78 mmol) of Fmoc-Cys(Trt)-OH was activated by adding 439 mg (1.16 mmol) of HBTU and 50 μL(0.28 mmol) of DIPEA in 2 mL DMF. After incubating for 20 min, 100 mg (0.39 mmol) of biotin-hydrazide dissolved in 1 mL DMSO was added dropwise. The reaction mixture was stirred at room temperature overnight. Then, excess diethyl ether (Sigma) was added to the reaction to make seperated two layers. After removing the upper layper, ethyl acetate (Sigma) was added to the yellow lower layer to precipitate out **5**. Deprotection of Fmoc was performed by incubation of **5** for 30 min in 10% v/v piperidine in DMF followed by precipitation using diethyl ether. Then, Trt group was removed by incubation of the precipitation from last step in TFA/DCM (1:1) mixture in the presence of 5 molar equivalent of triethylsilane (TES) (Sigma, 97%) for 1 h. The product (NH_2-Cys-biotin) was precipitated out using diethyl ether and washed at least five times. The washed product was dissolved in DMF, and DIPEA was added until pH reaches at ~8. 1.5 times molar excess of 2,2-dithiodipyridine (Sigma) dissolved in DMF was added. The reaction mixture was stirred for 2 h at room temperature and **6** was precipitated out using diethyl ether. **6** was dissolved in DMF and added slowly to 1.5 times molar excess of 2,2,5,5-tetramethyl-3-pyrrolin-1-oxyl-3-carboxylic acid (Acros Organics, 99%) whose carboxylic group was activated with 1.5 times molar excess of HBTU and 1 molar equivalent of DIPEA. The reaction was stirred at room temperature for 3 h. The final product, **2** was precipitated out as white powder using diethyl ether and washed several times. **2** was analyzed by electron spray ionization (ESI) mass spectrometry (Xevo G2-S QTof, Waters). Exact Mass of M+H is 637.2167 and the actual peak was at 637.2178. Total yield was about 20%.

b. ESI-Mass analysis of BtnRG-TP

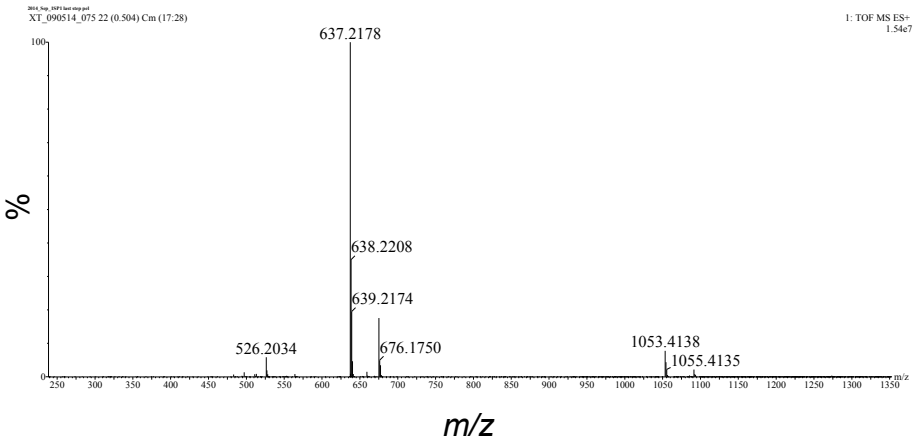

c. ESI-Mass analysis of compound 6

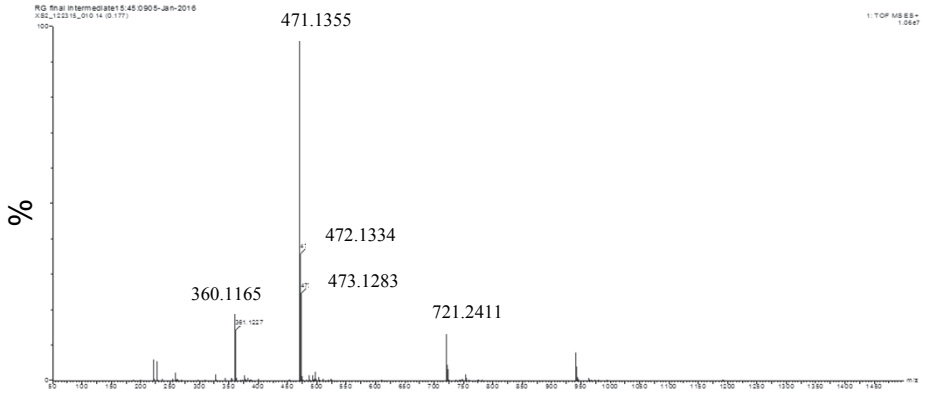

d. Note on the structural analysis of BtnRG-TP using NMR

Due to the paramagnetic relaxation enhancement by 2,2,5,5-tetramethyl-3-pyrrolin-1-oxyl group in BtnRG-TP, sufficiently high intensity and resolution of ^{1}H NMR spectrum could not be obtained. We, therefore, used indirect method to guide the NMR assignment of BtnRG-TP: NMR spectrum of compound **6** (the precursor to which the spin label was conjugated) was assigned first, then, the NMR spectrum of both compounds were aligned to determine the common peaks between compound **6** and **BtnRG-TP** (final product) as well as the additional proton signals from 2,2,5,5-tetramethyl-3-pyrrolin-1-oxyl group in BtnRG-TP. Those additional signals originated from methyl groups (1.43-1.30 ppm) and a beta proton (7.26 ppm) of 2,2,5,5-tetramethyl-3-pyrrolin-1-oxyl group. Moreover, the proton signal at 3.01 ppm in compound **6** shifted to 3.20 ppm, indicating the addition of 2,2,5,5-tetramethyl-3-pyrrolin-1-oxyl group to the amine group of the compound **6**. The intensity and resolution of the ^{13}C NMR spectrum of BtnRG-TP was even poorer than that of ^{1}H NMR. Therefore, ^{13}C NMR was not pursued further and ^{13}C NMR for compound **6** is shown below.

e. ^{1}H NMR analysis of compound 6

^{1}H NMR (500 MHz, DMSO-d_6): δ8.50 – 8.35 (m, 1H), 7.86 – 7.75 (m, 2H), 7.30 – 7.17 (m, 1H), 4.49 (dd, *J* = 13.0, 5.3 Hz, 1H), 4.38 – 4.22 (m, 1H), 3.75 – 3.63 (m, 1H), 3.28 – 3.15 (m, 2H), 3.01 (dt, *J* = 13.8, 7.3 Hz, 1H), 2.96 – 2.87 (m, 1H), 2.70 (dd, *J* = 12.7, 2.7 Hz, 1H), 2.38 – 2.21 (m, 2H), 1.84 – 1.42 (m, 6H).

f. ^{1}H NMR analysis of BtnRG-TP

^{1}H NMR (500 MHz, DMSO-d_6): δ 8.42 (s, 1H), 7.82 (s, 2H), 7.26 (d, *J* = 27.6 Hz, 2H), 4.47 (s, 1H), 4.30 (s, 1H), 3.72 (dt, *J* = 13.2, 6.6 Hz, 2H), 3.27 – 3.13 (m, 3H), 2.92 (d, *J* = 9.5 Hz, 1H), 2.69 (d, *J* = 12.5 Hz, 1H), 2.26 (s, 2H), 1.84 – 1.41 (m, 6H), 1.43 – 1.30 (m, 12H).

g. ^{13}C NMR analysis of compound 6

^{13}C NMR (126 MHz, DMSO-d_6): δ 171.05, 163.12, 159.49, 150.03, 138.29, 121.63, 119.96, 61.45, 59.62, 55.85, 53.23, 39.68, 39.51, 33.33, 28.51, 28.46, 25.49.